Soft Matter

Accepted Manuscript

ROYAL SOCIETY OF CHEMISTRY

www.rsc.org/softmatter

Universal scaling of crowding-induced DNA mobility is coupled with topology-dependent molecular compaction and elongation

Stephanie M. Gorczyca,[a] Cole D. Chapman,[b] and Rae M. Robertson-Anderson*[a]

[a.] *Department of Physics, University of San Diego, 5998 Alcala Park, San Diego, CA 92110 USA.*
[b.] *Department of Physics, University of California San Diego, 9500 Gilman Drive, La Jolla, CA 92093 USA.*
Email: randerson@sandiego.edu

Abstract

Using single-molecule fluorescence microscopy and particle-tracking techniques, we elucidate the role DNA topology plays in the diffusion and conformational dynamics of crowded DNA molecules. We focus on large (115 kbp), double-stranded ring and linear DNA crowded by varying concentrations (0-40%) of dextran (10, 500 kDa) that mimic cellular conditions. By tracking the center-of-mass and measuring the lengths of the major and minor axes of single DNA molecules, we characterize both DNA mobility reduction as well as crowding-induced conformational changes (from random spherical coils). We reveal novel topology-dependent conformations, with single ring molecules undergoing compaction to ordered spherical configurations ~20% smaller than dilute random coils, while linear DNA elongates by ~2-fold. Surprisingly, these highly different conformations result in nearly identical exponential mobility reduction dependent solely on crowder volume fraction Φ, revealing a universal critical crowding concentration of $\Phi_c \cong 2.3$. Beyond Φ_c DNA exhibits topology-independent conformational relaxation dynamics despite highly distinct topology-driven conformations. Our collective results reveal that topology-dependent conformational changes, unique to crowded environments, enable DNA to overcome the classically expected mobility reduction that high-viscosity crowded environments impose. Such coupled universal dynamics suggest a mechanism for DNA to maintain sufficient mobility required for wide-ranging biological processes despite severe cellular crowding.

Introduction

DNA naturally occurs in both relaxed circular (ring) and linear topologies, with long molecules – kilobasepairs (kbp) to mega kbp in length – forming the genomes of eukaryotic and prokaryotic cells, respectively. Within biological cells, these large DNA molecules are forced to function in highly crowded environments of other macromolecules, with concentrations of ~200-400 mg/ml (20-40%).[1] This ubiquitous crowding hinders DNA mobility and can induce conformational changes that directly impact a wide range of biological processes, including replication, transcription, chromosomal compaction, DNA looping, gene expression and delivery, and transfection and transformation.[1-8] Ring and linear DNA have been shown to exhibit highly varying dynamics in both dilute and concentrated DNA solutions,[3, 4, 9-17] yet both topologies must perform similar functions in the cell. Ring DNA is of specific interest as circular plasmids are used widely for introducing genes into cells to increase antibiotic resistance.[18] Despite the widespread importance and relevance of crowding-induced DNA dynamics,[1, 3, 4, 8, 10, 12, 17, 19] how crowding affects topologically distinct DNA remains an open question. Beyond the obvious biological importance, elucidation of this question is essential to advancements in the design of specific drug delivery systems and gene therapy techniques that use ring versus linear DNA;[3, 4, 20] as well as fabrication of multifunctional biomaterials and artificial cells.

We previously found remarkably large differences between ring and linear DNA mobility in entangled DNA solutions with a complex dependence on solution concentration as well as topology of both the diffusing molecule and those entangling it.[21-23] Namely, isolated rings or those entangled by other ring DNA diffused ~1.3x faster than linear DNA, but when entangled with linear chains, the mobility of rings was reduced ~10x more than diffusing linear DNA.[24] Several simulations[11, 13, 16, 25] and synthetic polymer experiments[26-29] have investigated mobility of concentrated ring and linear polymers reporting topology-dependent results similar to ours, which are generally understood to be due to threading of rings by surrounding linear chains.

Several previous studies have also found evidence of topology-dependent DNA and polymer conformations in concentrated solutions, reporting varied and conflicting results.[9, 11, 13-15, 30] While simulations[13-15] have reported evidence of concentrated rings collapsing whereas linear chains maintain random coil configurations, other groups have shown these rings actually swell beyond their dilute size and adopt more aspherical or elongated configurations.[9, 30] Simulation studies have also reported evidence of ring compaction when concentrated by other rings, but swelling when surrounded by linear chains due to threading.[11, 15]

Macromolecular crowding adds a layer of complexity to the phase space of concentrated polymer solutions as the surrounding polymers are distinct in size, shape and structure from the diffusing polymer of interest (here large ring and linear DNA). We previously showed that for linear DNA (11, 115 kbp) in in-vitro crowded environments (0-40% w/v dextran solutions), crowding-induced mobility reduction was independent of DNA length and solely mediated by crowder size and concentration.[10] While the mobility of DNA was reduced with increasing crowding, DNA actually diffused faster than classically predicted by the Stokes-Einstein relation ($D \sim \eta^{-1}$) for increasingly viscous dextran solutions. We also revealed novel crowding-induced dynamic elongation states of single DNA random coils, which we understand to be due to entropic effects. Specifically, to maximize the available volume (and thus entropy) of the crowders, thin DNA molecules are driven to elongate into lower entropy, smaller volume states. For reference, the random coil volume of 115 kbp DNA is ~1 μm^3 compared to a volume of ~10^{-4} μm^3 for a fully elongated strand. While compaction would also reduce crowder excluded volume, perhaps even

more effectively, and has been reported for linear DNA in certain crowding conditions,[12, 17, 31, 32] the energetic cost of charge repulsion of DNA strands at the physiological salt concentrations used in our experiments prohibits such conformations.

Enhanced mobility coupled with elongation for linear DNA suggests that this conformational change, while lowering DNA entropy, facilitates mobility through the crowded cell. These findings raise the question: Is there a similar mechanism that rings can access to facilitate mobility in the cell? Ring DNA could potentially elongate from a random coil configuration by flattening to allow the two halves of the molecule to align with each other. However, this conformation, compared to elongated linear DNA, is expected to be prohibitively costly due to the added electrostatic energy of two negatively charged strands in close proximity, as well as large bending energies at the ends. Thus, can ring DNA exhibit enhanced mobility when crowded? If so, what conformational change, if any, allows for this mobility? While there have been numerous studies investigating the impact of crowding on macromolecular dynamics and conformations, there are surprisingly few studies devoted to crowded ring polymers or the impact of topology on crowded DNA.[33] Thus, these important questions have remained unanswered.

Here, we elucidate the complex issues and questions outlined above by using fluorescence microscopy and robust particle-tracking and image analysis techniques to characterize the diffusion and conformational dynamics of long ring DNA in in-vitro crowded solutions of dextran (10, 500 kDa). We reveal novel dynamic compaction of ring DNA and enhanced DNA mobility that is surprisingly independent of molecular topology. Our collective results uncover the topologically-dependent underlying molecular dynamics and properties that drive DNA mobility, conformation and function in complex crowded cell-like environments and biomaterials.

Methods and Materials

Double-stranded supercoiled DNA (115 kbp) is prepared via replication of bacterial artificial chromosome constructs in Escherichia coli, followed by extraction and purification as described previously.[21, 34] Supercoiled DNA is converted to ring (relaxed circular) and linear topologies via treatment with topoisomerase-I and MluI (New England Biolabs), respectively.[24] All subsequent sample preparation, data collection and analysis techniques are depicted and described in Figure 1. For measurements, a trace amount of DNA, uniformly labeled with YOYO-I (Invitrogen), is embedded in solutions of 0-40% w/v dextran (10 or 500 kDa; Sigma) dissolved in aqueous buffer (10 mM Tris-HCl, 1 mM EDTA, 10 mM NaCl, 4% β-mercaptoethanol). Dextran serves as the crowder in our experiments, as it is a commonly used inert crowder similar to the size of biological proteins in the cell.[17, 35, 36] Dextran solution viscosities were measured using optical tweezers as described previously.[10]

DNA-dextran solutions are loaded into a microscope sample chamber, equilibrated, and then imaged using a high speed CCD QImaging camera on a Nikon Eclipse A1R inverted microscope with a 60X objective. For each crowding condition, ~200 molecules are imaged for 30 seconds each at a rate of 10 frames per second. Using our previously established[10] custom-written software (Matlab), we measure and track the center of mass (COM) position and lengths of the major axis (R_{max}) and minor axis (R_{min}) of each molecule in each frame (measurement techniques described in more detail in Ref 10). We calculate diffusion coefficients from COM mean squared displacements (i.e. $\langle(\Delta x)^2\rangle = \langle(\Delta y)^2\rangle = 2Dt$). Using measured R_{max} and R_{min} values we also quantify molecular elongation $E = (R_{max}/R_{min}) - 1$. To determine the time dependence of conformational states, we also calculate the ensemble averaged fluctuation length

$L(t) = \langle|R_{max}(0) - R_{max}(t)|\rangle$ which quantifies the lengthscale over which individual DNA molecules conformationally fluctuate.

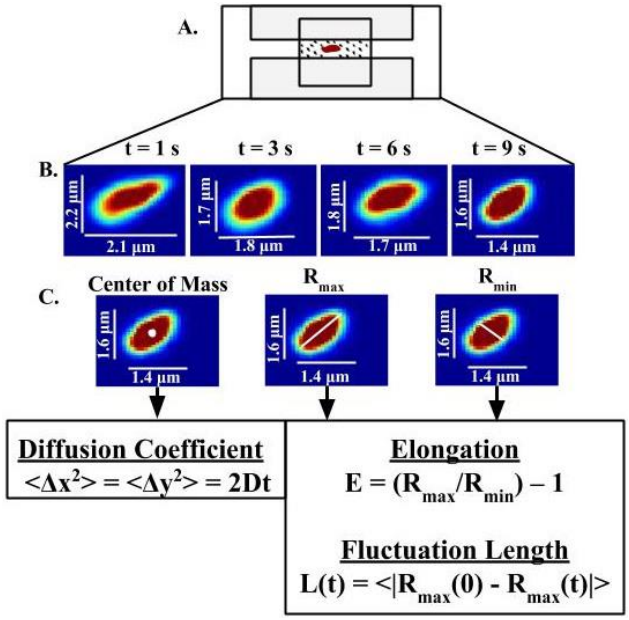

Figure 1: Experiment Schematic. (A) A trace amount of YOYO-I-labeled 115 kbp DNA, embedded in a crowded solution of 0-40% w/v dextran (10 or 500 kDa) is loaded into a sample chamber, sealed, and equilibrated. (B) Single embedded DNA molecules are imaged for ~30 seconds at 10 fps with a high speed CCD QImaging camera on a Nikon Eclipse A1R inverted microscope with a 60X objective. (C) To quantify DNA mobility and conformational dynamics the center of mass position (x,y) and lengths of major and minor axes, R_{max} and R_{min}, are measured and tracked in time t. Measured quantities are used to quantify the molecular diffusion coefficient (D), elongation (E), and fluctuation length (L) via the displayed equations.

Results and Discussion

Diffusion

We first characterize the impact of DNA topology, crowder size and crowder concentration on DNA diffusion, and compare our measured diffusion coefficients to those classically predicted provided the viscosity of dextran solutions (i.e. $D \sim \eta^{-1}$) (Fig 2). Our measured diffusion coefficients for ring and linear DNA display remarkably similar effects of crowding concentration on mobility reduction. As displayed in Figure 2, the mobility reduction appears completely independent of DNA topology, driven solely by crowding conditions. Such similarity is surprising given the large differences reported between the mobility of ring and linear polymers (including DNA) in entangled and complex crowded environments.[22 11, 13, 16, 25] Furthermore, DNA diffusion is actually faster than expected from the increasing viscosity of the dextran solutions (Fig 2 inset), as we previously reported for crowded linear DNA of varying lengths.[10] To determine whether the dependence on crowder size is due to differences in crowder mobility or volume occupied by different sizes of dextran, we normalize dextran concentrations by the overlap concentration for each crowder ($C^* \cong (M/N_A)/(4\pi/3)R_G^3$ where the radii of gyration R_G are 3.5 nm and 19 nm for 10 kDa and 500 kDa dextran respectively[37]) to express concentrations in terms of the volume fraction Φ of crowders in solution. Note that $\Phi > 1$ indicates that crowders are overlapping. As seen in Figure 2B, upon converting concentrations to volume fraction, all DNA diffusion coefficients

collapse onto a single universal curve. Mobility of both ring and linear chains is exponentially suppressed with increasing crowder volume fraction, i.e. $D \approx D_0 \exp(-\Phi/\Phi_c)$, revealing a critical volume fraction of $\Phi_c \cong 2.3$ necessary for substantive non-classical crowding effects on mobility. Thus, DNA mobility reduction in crowded environments is solely driven by the reduction in available solution volume for DNA rather than the size, mobility or number of crowders. This finding appears universal for DNA of varying topologies as well as varying lengths.[10] Furthermore, our measured critical volume fraction Φ_c, corresponding to 9.4% and 2.9% for small and large dextran, is below physiologically relevant cellular concentrations, suggesting that this universal nonclassical scaling is important to DNA function in cellular environments. We note that this novel result conflicts with previous simulation studies that find that crowders of varying size at equal volumes fractions affect both mobility and conformational changes differently.[33, 38] However, in these studies the size of crowders and tracked polymers are more comparable to each other than in our experiments where the R_G of dextran is >100x smaller than that of DNA.

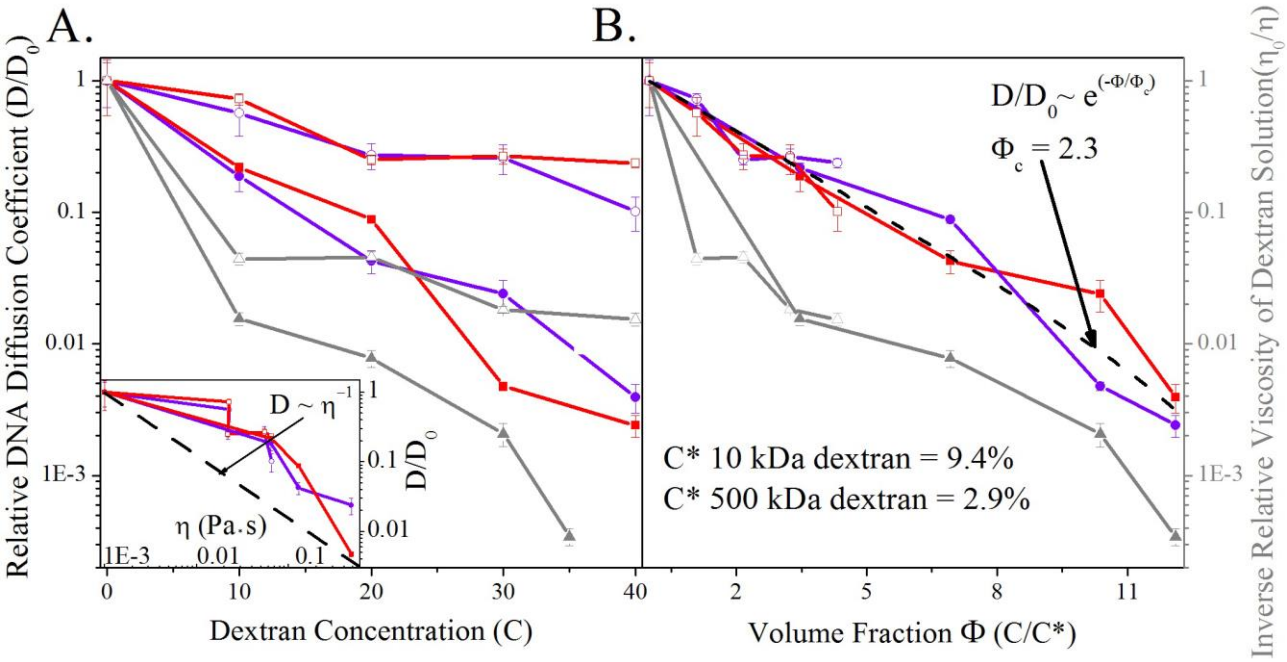

Figure 2: Crowding-induced mobility reduction of ring and linear DNA. DNA diffusion coefficients (D), normalized by respective 0% values (D_0), and inverse normalized viscosity of dextran solutions, η_0/η (*gray*), versus (A) dextran concentration, C (*% w/v*), and (B) volume fraction, Φ, for ring (*purple circles*) and linear (*red squares*) DNA in 10 kDa dextran (*open symbols*) and 500 kDa dextran (*closed symbols*). Remarkably, all DNA and crowder combinations exhibit the same exponential mobility reduction with increasing Φ. This universal scaling reveals a critical volume fraction Φ_c = 2.3 for substantial crowding-induced mobility reduction of DNA. Note that DNA mobility is faster than expected from the classical Stokes-Einstein relation $D \sim \eta^{-1}$ (*inset*). Viscosity data and most linear DNA data are reproduced from Ref 10.

As described in the Introduction, we previously interpreted the enhanced mobility for crowded linear DNA, as due to the conformational changes induced by crowding. Particularly, linear DNA molecules elongate from dilute random coil configuration upon crowding to aid mobility through crowders. Our universal crowding-induced mobility reduction suggests that rings must be undergoing similar conformational changes to facilitate movement through crowder obstacles. However, because the

ends of ring DNA chains are connected, the maximum elongation possible is only half that of their linear counterparts, and such elongated conformations would be significantly more energetically costly (requiring close alignment of two negatively charged strands as well as significant chain bending). To elucidate this seeming contradiction, we characterize the conformational dynamics of ring DNA upon crowding in comparison to linear DNA.

Conformation

As described in Methods, we measure and track the major axis, R_{max}, and minor axis, R_{min}, of ring DNA to quantify the impact of crowding on DNA conformational size (i.e. R_{max}) and elongation from spherical conformation ($E = R_{max}/R_{min} - 1$) (Fig 3). Surprisingly, crowding appears to induce nearly opposite conformational changes in rings compared to linear DNA as demonstrated by the probability distributions of R_{max} and E displayed in Figure 3. Ring DNA displays compaction, shown by a ~20% reduced R_{max} (Fig 3A) with little change to overall shape (i.e. no change in E) (Fig 3B), in stark contrast to linear DNA elongation (E values increased >5x and R_{max} values increased 30%). However, the population of both compacted rings and elongated linear chains only becomes substantial after ~$2\Phi_C$, coupling conformational changes to the critical excluded volume necessary for crowding-induced mobility reduction. Further, while the distribution of conformational states broadens with linear chain elongation, with the standard deviations σ of E and R_{max} values increasing by >3-fold and ~2-fold, respectively, the spread (σ) in R_{max} and E values for rings remains relatively unchanged (Fig 3, right panels). The significantly increased number of linear DNA elongation states, as compared to dilute random coils and compacted rings, indicates a more disordered spread in population dynamics induced by crowding.

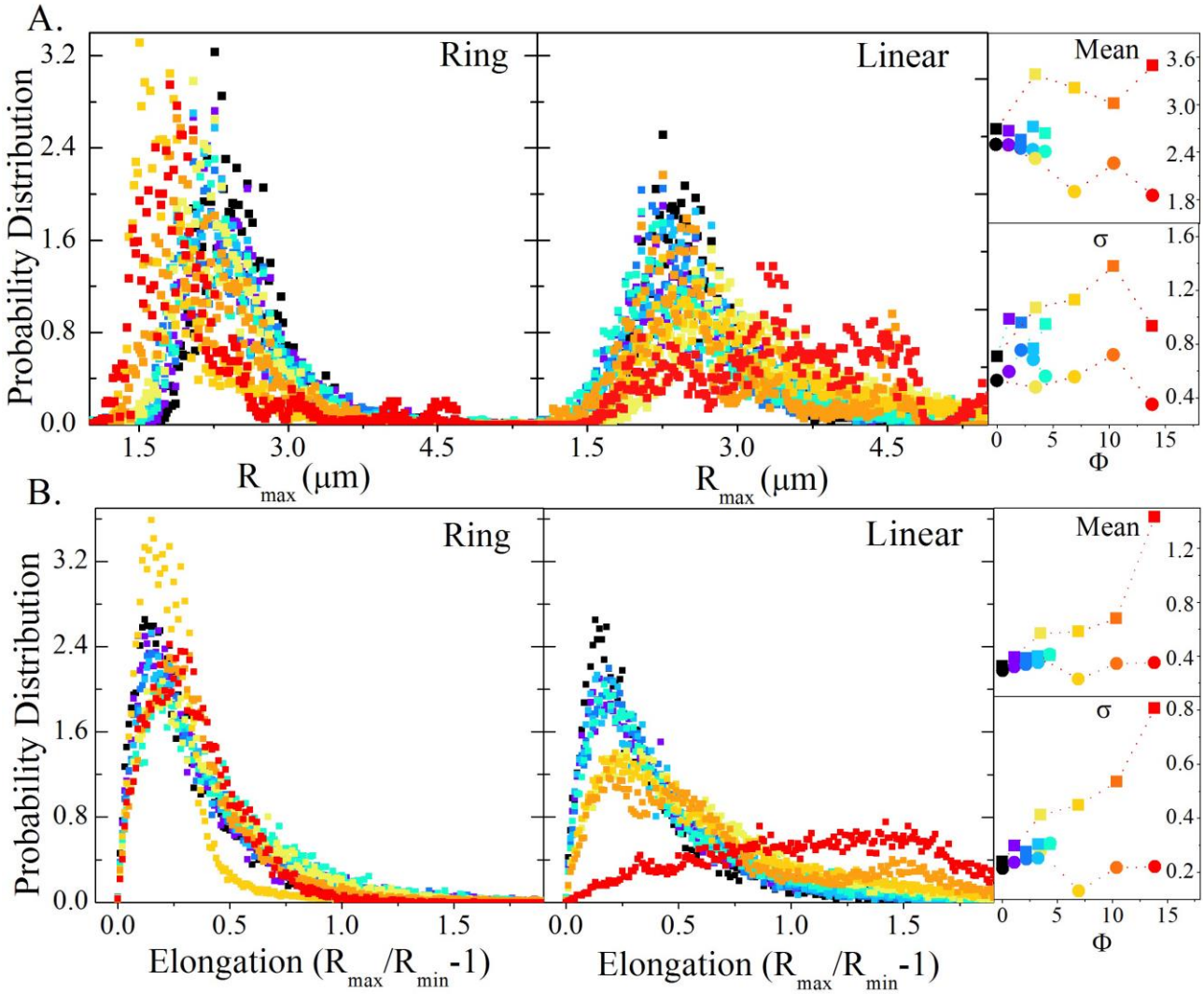

Figure 3: Crowding induces compaction of ring DNA and elongation of linear DNA. Probability distributions for the (A) major axis length R_{max} and (B) elongation parameter E for ring (left) and linear (right) DNA in 0-40% 10 kDa (*cold colors)* and 500 kDa (*warm colors)* dextran. Distributions for Φ = 0 (*black*), 1.1 (*purple*), 2.2 (*blue*), 3.2 (*light blue*), 4.3 (*light green*), 3.5 *(yellow*), 6.9 (*light orange*), 10.4 (*orange*), 13.8 (*red*) are shown. Right panels show the mean and standard deviation (σ) for each distribution with the same color/symbol scheme. As shown, ring minimal shape change (change in E) from spherical random coil. Linear DNA, on the other hand, elongates upon crowding by ~2-fold, sampling an increased range of conformational states (increasing σ). Conformational changes for both DNA topologies are only apparent for volume fractions >2Φ_C. Most raw data for linear DNA is the same as that from Ref 10.

To elucidate the time-dependence of this displayed topology-dependent spread in DNA conformations, we quantify the lengthscale of fluctuations *L(t)* between different conformational states and the corresponding relaxation timescales (Fig 4). In other words, we sought to determine whether the distributions of conformational states (Fig 3A) arise from an ensemble of individual molecules, each with relatively fixed conformational states that varied from molecule to molecule, or from individual molecules (all in similar states) fluctuating between different states in time. As described in Methods, the

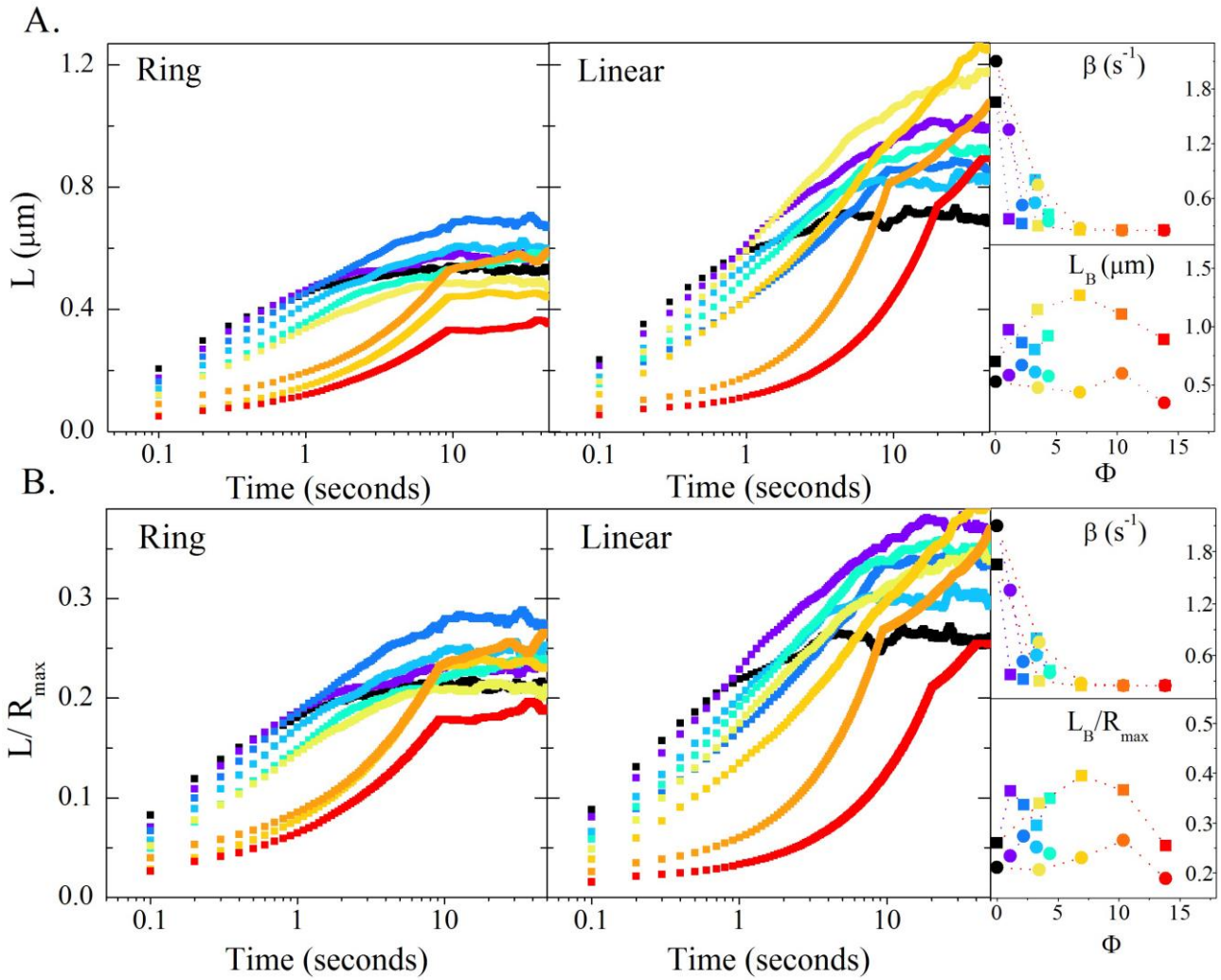

Figure 4: Crowded ring and linear DNA fluctuate between conformational states on equal timescales but over topology-dependent lengthscales. (A) Ensemble-averaged fluctuation length (L) and (B) fractional fluctuation length (L/R_{max}) vs. time for ring and linear DNA. Fluctuation length curves for all crowding concentrations (Φ = 0 to 13.8) for each DNA topology are shown with the same color scheme as Figure 3. Fluctuation lengths for all cases exponentially approach maximal fluctuation or "breathing" lengths L_B between different conformational states at rates β (right panels). Maximal breathing lengthscales L_B for ring DNA decrease by 36% upon crowding, demonstrating ordered compaction, while linear DNA L_B increases by 27% indicating broadly distributed elongation states. Relaxation rates for both topologies, differing by ~1.3x in the dilute case, both drop to an identical fluctuation rate of 0.25 s^{-1} for all volume fractions Φ exceeding ~6 (~2.5Φ_c). This topology-independent rate is surprisingly robust to further increases in Φ. Most raw data for linear DNA is the same as that from Ref 10.

fluctuation length ($L(t) = \langle|R_{max}(0) - R_{max}(t)|\rangle$) quantifies how quickly the conformational state of a molecule is changing and the corresponding lengthscale of conformational fluctuations or "breathing" between different states. Explicitly, the fluctuation length measures the difference between the magnitude of the major axis of the DNA molecule in time t and the major axis length at t = 0. Thus we expect $L(t)$ to grow from 0 to a maximal value (L_B) reflecting the spread in conformational states accessed by each molecule or the lengthscale of conformational breathing (as seen in Fig 4). This lengthscale L_B is

comparable to the standard deviation of the R_{max} distributions in Fig 3A, demonstrating that the spread in conformational states is in fact due to each molecule conformationally breathing between different states as it diffuses. Each fluctuation length approaches L_B exponentially in time at a breathing rate β that measures how quickly DNA molecules are changing conformational size or shape as they diffuse (Fig 4A). Both L_B and β are determined via single-exponential fits to each L (R^2 values are 0.89 – 0.97 with a mean of 0.95).

In the dilute case, rings fluctuate ~1.3x faster (Fig 4, right panels) over ~1.3x smaller length scales (L_B) than linear DNA, as expected provided the ~1.3x faster diffusion of dilute ring DNA, with a correspondingly reduced radius of gyration.[24] However, upon crowding, fluctuation relaxations of both ring and linear DNA are slowed to a topology-independent rate of $\beta \cong 0.25$ s^{-1} at ~2.5Φ_C (Fig 4, right panels). This topology-independent fluctuation timescale, which further corroborates our universal mobility reduction results, is surprisingly robust to further increases in crowding concentrations. Interestingly, this topology-independent relaxation is coupled with starkly different changes in fluctuation length scales for rings compared to linear chains. For volume fractions above ~2Φ_C, the maximal fluctuation length of ring DNA is reduced by 36%, in support of a reduction in DNA size (compaction), while linear DNA fluctuations display an 81% increase in L_B, supporting elongation.

This crowding-induced change in fluctuation lengthscales could be solely a result of decreasing and increasing sizes or lengthscales of ring and linear DNA, with the fractional extent of fluctuations remaining constant relative to conformation size. However, these changes could also indicate that the lengthscale of fluctuations relative to the DNA size is increasing or decreasing, suggesting a mechanism for altered mobility characteristics. To delineate between these two effects, we normalize fluctuation lengths $L(t)$ by the maximum lengthscale of DNA conformations (R_{max}), to quantify the fractional fluctuation length of DNA (Fig 4B). We find that the drastic topology-dependent changes in $L(t)$ largely disappear upon this normalization, with all L/R_{max} values for rings and linear chains increasing or remaining unchanged from the dilute case. Thus, the reduction in L_B for rings does indeed indicate compaction (reduction in DNA size) rather than reduced conformational fluctuations. Furthermore, the crowding-induced increase in fractional fluctuation lengths (most apparent for linear DNA with an increase from ~0.25 to 0.35) indicates that while crowding forces slower molecular movements (both COM diffusion and conformational relaxation), each movement is larger, offsetting extreme viscosity-driven slowing. In other words, while the time scale of random walk "steps" DNA takes is longer, the step size is also increased, reducing the drastic slowing classically predicted by increasing the step timescale of a random walk.

We note that the increase in L/R_{max} is actually nonmonotonic with volume fraction, increasing until $\Phi \approx 8$ then decreasing again. We can understand this nonmonotonic variation in fractional conformational breathing as due to reduced microscale variations in the crowding mesh once crowder concentrations are well above the overlap concentration ($\Phi \geq 10$). For volume fractions on the order of 1 the crowders are, on average, just barely overlapping, leading to likely microscopic inhomogeneities in the network with the DNA encountering regions of overlapping mesh and regions of discrete, non-overlapping crowders (with these regions changing in time due to the mobility of the crowders). Diffusion through microscopically varying environments leads DNA to undergo larger scale fluctuations between conformational states. In other words, the distribution of crowding environments will cause DNA to access a larger distribution of conformational states (also reflected in the non-monotonicity of the standard deviation of R_{max} distributions). However, for $\Phi \geq 10$, the environment the DNA diffuses through

is a uniform mesh with likely little variation. Thus, the DNA can access a smaller range of free energy minimizing conformational states as it diffuses through different regions of the homogenous crowding network (Fig 4, bottom right panel). This nonmonotonicity can also explain why the COM diffusion coefficients continue to decrease with increasing volume fraction while the conformational breathing rates remain unchanged beyond ~$2.5\Phi_C$.

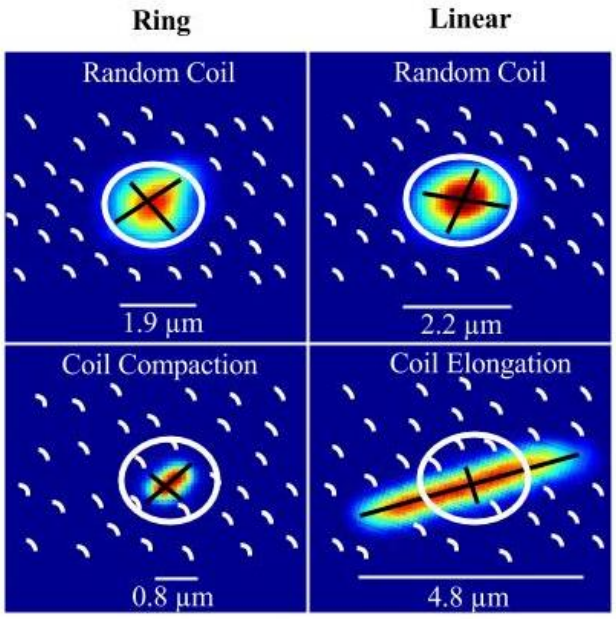

Figure 5: Entropically-driven compaction and elongation of ring and linear DNA in crowded environments. Microscope images of typical fluorescent-labeled ring and linear DNA conformations in both dilute solutions (top panels) and crowded dextran solutions (bottom panels). Crowders (dextran) are depicted as *white marks* in the dilute as well as crowded environments to illustrate the ability of crowders to spread out more when DNA compacts or elongates. DNA random coils (top), the maximum entropy conformation for ring and linear DNA diffusing in dilute solutions, take up substantial volume in crowded solutions that crowders cannot access (*white circle*). To minimize this excluded volume, thereby maximizing crowder entropy, DNA undergoes topology-dependent conformational changes. Ring DNA undergoes ~20% compaction while linear DNA elongates by ~2-fold. The two highly distinct conformational changes lead to surprisingly similar transport (see Fig 2).

We previously explained crowding-induced elongation of linear DNA as due to entropic excluded volume effects. As described in the Introduction, smaller volume compacted states, which could provide even more volume for crowders to access than elongated states, was understood to be prohibitively costly due to electrostatic repulsion of neighboring DNA segments. So why then can ring DNA compact in the same conditions? As described in the Introduction, because ring DNA has no free ends, any attempt to conformationally elongate would come with an electrostatic cost (as well as bending energy cost) not felt by linear chains. Thus, no volume-minimizing conformation is allowable for ring DNA that does not come with an energetic cost. Because crowder entropy (i.e. volume) maximization is still the driving force behind the conformational change, and both volume-minimizing conformations come with an electrostatic cost for ring DNA, rings will convert to whichever conformation provides more gain in crowder volume. Thus, ring DNA undergoes compaction, reducing the conformational volume to ~47% of the random coil

excluded volume, while linear chains elongate, with a less extreme volume reduction to ~66% of the corresponding dilute coil volume (Fig 5). Both conformations, while lowering the configurational entropy of DNA, aid molecular transport through crowders. While ring DNA compaction results in smaller, tighter conformations that can diffuse faster through crowders than random coils, elongated linear chains can take larger Brownian steps than random coils (Fig 4B). Non-classical coupling of DNA transport and conformation, unique to crowded environments, has also recently been reported for DNA hairpin looping kinetics in which viscosity alone can only slow looping kinetics while crowding is needed to alter the steady-state populations of hairpins.[7]

Conclusion

In conclusion, we use single-molecule fluorescence microscopy and particle-tracking techniques to show, for the first time, that long ring and linear DNA in cellular crowding conditions, undergo universal enhanced diffusion, independent of DNA topology and length as well as crowder size. This universal exponential scaling of mobility is entropically driven solely by the solution volume taken up by increased concentrations of crowders. We further find that conformational relaxation rates of DNA are equally universal reaching a crowding-induced rate of ~0.25 s^{-1} independent of DNA topology and size. We show that this enhanced topology-independent mobility is coupled to nearly opposite conformational changes for ring and linear DNA, with rings undergoing compaction while linear DNA elongates. Together, our diffusion and conformational dynamics results reveal a critical crowding volume fraction of $\Phi_c \cong 2.3$ necessary for such topology-independent mobility coupled with topology-driven conformational changes of large crowded DNA. Our findings reveal mechanisms by which DNA and other macromolecules, with both closed and free ends, can access different conformational states to achieve similarly efficient mobility in cellular environments. As such, our results elucidate a wide range of biological processes in both bacterial and eukaryotic cells, including replication, transcription, and a myriad of DNA-protein binding events. Furthermore, our results are essential to the optimal design of advanced gene therapy and drug delivery techniques, as well as new biomimetic materials and artificial cells.

Acknowledgements

This research was funded by the AFOSR Young Investigator Program, Grant No. FA95550-12-1-0315 and the Arnold and Mabel Beckman Scholarship Foundation.

References

1. R. J. Ellis, *Current opinion in structural biology*, 2001, **11**, 114-119.
2. G. W. Li, O. G. Berg and J. Elf, *Nat Phys*, 2009, **5**, 294-297.
3. D. Miyoshi and N. Sugimoto, *Biochimie*, 2008, **90**, 1040-1051.
4. S. Nakano, D. Miyoshi and N. Sugimoto, *Chemical reviews*, 2014, **114**, 2733-2758.
5. J. Pelletier, K. Halvorsen, B.-Y. Ha, R. Paparcone, S. J. Sandler, C. L. Woldringh, W. P. Wong and S. Jun, *Proceedings of the National Academy of Sciences*, 2012, **109**, E2649-E2656.
6. G. Rivas, F. Ferrone and J. Herzfeld, *EMBO reports*, 2004, **5**, 23-27.
7. O. Stiehl, K. Weidner-Hertrampf and M. Weiss, *New Journal of Physics*, 2013, **15**, 113010.
8. C. Tan, S. Saurabh, M. P. Bruchez, R. Schwartz and P. LeDuc, *Nature nanotechnology*, 2013, **8**, 602-608.
9. F. Benedetti, A. Japaridze, J. Dorier, D. Racko, R. Kwapich, Y. Burnier, G. Dietler and A. Stasiak, *Nucleic acids research*, 2015, **43**, 2390-2399.

10. C. D. Chapman, S. Gorczyca and R. M. Robertson-Anderson, *Biophysical journal*, 2015, **108**, 1220-1228.
11. S. F. Henke and S. Shanbhag, *React Funct Polym*, 2014, **80**, 57-60.
12. M. Kojima, K. Kubo and K. Yoshikawa, *The Journal of chemical physics*, 2006, **124**, 024902.
13. M. Muller, J. P. Wittmer and M. E. Cates, *Phys Rev E*, 2000, **61**, 4078-4089.
14. S. Y. Reigh and D. Y. Yoon, *Acs Macro Lett*, 2013, **2**, 296-300.
15. G. Subramanian and S. Shanbhag, *Physical review. E, Statistical, nonlinear, and soft matter physics*, 2008, **77**, 011801.
16. G. Subramanian and S. Shanbhag, *Macromolecules*, 2008, **41**, 7239-7242.
17. C. Zhang, P. G. Shao, J. A. van Kan and J. R. van der Maarel, *Proceedings of the National Academy of Sciences of the United States of America*, 2009, **106**, 16651-16656.
18. P. M. Bennett, *British journal of pharmacology*, 2008, **153 Suppl 1**, S347-357.
19. R. de Vries, *Polymer Science Series C*, 2012, **54**, 30-35.
20. J. K. Vasir and V. Labhasetwar, *Expert Opin Drug Del*, 2006, **3**, 325-344.
21. C. D. Chapman, S. Shanbhag, D. E. Smith and R. M. Robertson-Anderson, *Soft Matter*, 2012, **8**, 9177-9182.
22. R. M. Robertson and D. E. Smith, *Macromolecules*, 2007, **40**, 3373-3377.
23. R. M. Robertson and D. E. Smith, *Proceedings of the National Academy of Sciences*, 2007, **104**, 4824-4827.
24. R. M. Robertson, S. Laib and D. E. Smith, *Proceedings of the National Academy of Sciences*, 2006, **103**, 7310-7314.
25. D. Michieletto, M. Baiesi, E. Orlandini and M. S. Turner, *Soft Matter*, 2015, **11**, 1100-1106.
26. T. Cosgrove, M. Turner, P. Griffiths, J. Hollingshurst, M. Shenton and J. Semlyen, *Polymer*, 1996, **37**, 1535-1540.
27. G. McKenna, G. Hadziioannou, P. Lutz, G. Hild, C. Strazielle, C. Straupe, P. Rempp and A. Kovacs, *Macromolecules*, 1987, **20**, 498-512.
28. D. Orrah, J. Semlyen and S. Ross-Murphy, *Polymer*, 1988, **29**, 1452-1454.
29. S. Tead, E. Kramer, G. Hadziioannou, M. Antonietti, H. Sillescu, P. Lutz and C. Strazielle, *Macromolecules*, 1992, **25**, 3942-3947.
30. M. Bernabei, P. Bacova, A. J. Moreno, A. Narros and C. N. Likos, *Soft Matter*, 2013, **9**, 1287-1300.
31. B. R. Somalinga and R. P. Roy, *J Biol Chem*, 2002, **277**, 43253-43261.
32. D. Tsao and N. V. Dokholyan, *Physical chemistry chemical physics : PCCP*, 2010, **12**, 3491-3500.
33. J. Shin, A. G. Cherstvy and R. Metzler, *New Journal of Physics*, 2014, **16**.
34. S. Laib, R. M. Robertson and D. E. Smith, *Macromolecules*, 2006, **39**, 4115-4119.
35. I. Pastor, L. Pitulice, C. Balcells, E. Vilaseca, S. Madurga, A. Isvoran, M. Cascante and F. Mas, *Biophysical chemistry*, 2014, **185**, 8-13.
36. C. Benjamin Renner, N. Du and P. S. Doyle, *Biomicrofluidics*, 2014, **8**, 034103.
37. J. J. Jones, J. R. van der Maarel and P. S. Doyle, *Nano letters*, 2011, **11**, 5047-5053.
38. J. Kim, C. Jeon, H. Jeong, Y. Jung and B. Y. Ha, *Soft Matter*, 2015, **11**, 1877-1888.